Biochemistry and Biophysics Reports 26 (2021) 100983

Contents lists available at ScienceDirect

Biochemistry and Biophysics Reports

journal homepage: www.elsevier.com/locate/bbrep

Hyperglycemia and hyperlipidemia can induce morphophysiological changes in rat cardiac cell line

Rocío Varela [a], Inés Rauschert [a,b], Gerardo Romanelli [a], Andrés Alberro [a], Juan C. Benech [a,b,*]

[a] Laboratorio de Señalización Celular y Nanobiología, Instituto de Investigaciones Biológicas Clemente Estable (IIBCE), Av. Italia, 3318, CP, 11600, Montevideo, Uruguay

[b] Plataforma de Microscopía de Fuerza Atómica, Instituto de Investigaciones Biológicas Clemente Estable (IIBCE), Av. Italia, 3318, CP, 11600, Montevideo, Uruguay

ARTICLE INFO

Keywords:
Hyperglycemia
Hyperlipidemia
Cardiac cells
Actin cytoskeleton
Cell stiffness
Elasticity maps

ABSTRACT

H9c2 cardiac cells were incubated under the control condition and at different hyperglycemic and hyperlipidemic media, and the following parameters were determined and quantified: a) cell death, b) type of cell death, and c) changes in cell length, width and height. Of all the proven media, the one that showed the greatest differences compared to the control was the medium glucose (G) 33 mM + 500 μM palmitic acid. This condition was called the hyperglycemic and hyperlipidemic condition (HHC). Incubation of H9c2 cells in HHC promoted 5.2 times greater total cell death when compared to the control. Of the total death ofthe HHC cells, 38.6% was late apoptotic and 8.3% early apoptotic. HHC also changes cell morphology.

The reordering of the actin cytoskeleton and cell stiffness was also studied in control and HHC cells. The actin cytoskeleton was quantified and the number and distance of actin bundles were not the same in the control as under HHC. Young's modulus images show a map of cell stiffness. Cells incubated in HHC with the reordered actin cytoskeleton were stiffer than those incubated in control. The region of greatest stiffness was the peripheral zone of HHC cells (where the number of actin bundles was higher and the distance between them smaller).

Our results suggest a correlation between the reordering of the actin cytoskeleton and cell stiffness. Thus, our study showed that HHC can promote morphophysiological changes in rat cardiac cells confirming that gluco-and lipotoxicity may play a central role in the development of diabetic cardiomyopathy.

1. Introduction

Diabetes mellitus (DM) is one of the most prevalent metabolic disorders in the world. The International Diabetes Federation estimated that approximately 463 million adults aged 20–79 years suffered DM in 2019, and this number is expected to increase to 592 million by 2035 and 642 million by 2040 [1–3]. Data showed that DM caused more than 4.2 million deaths, and heart failure was a major contributor to the cardiovascular morbidity and mortality of these patients [4–6]. Rubler et al., 1972 [6] coined the term "diabetic cardiomyopathy" (DC) to characterize myocardial dysfunction in diabetic patients in the absence of coronary artery disease, hypertrophy, or valvular heart disease. The pathophysiology and underlying morphophysiological changes caused by heart failure in those patients remain largely unknown [7,8]. It is generally accepted and agreed upon that the pathogenesis of DC depends on several factors, some of which are autonomic dysfunction, metabolic derangements, abnormalities in ion homeostasis, changes in structural proteins, and interstitial fibrosis [9,10]. It has been shown that an early indication in diabetic myocardial dysfunction is the stiffening of the left ventricle [11–13], which is usually attributed to myocardial fibrosis and the accumulation of advanced glycation end products [14,15] Although, diastolic dysfunction can appear in DC before any significant accumulation of collagen [16].

Actin is a plentiful and essential cytoskeletal protein in eukaryotic cells. It plays an integral role in several cellular processes ranging from motility and contraction to intracellular transport, cytokinesis and adhesion [17,18]. Furthermore, many reports showed that actin cytoskeleton has a crucial effect in mechanical properties of different cell types [19–24] including cardiomyocytes [25–28]. In agreement with this evidence, it was found that live cardiomyocytes isolated from adult

* Corresponding author. Laboratorio de Señalización Celular y Nanobiología, Instituto de Investigaciones Biológicas Clemente Estable (IIBCE), Av. Italia, 3318, CP, 11600, Montevideo, Uruguay.

E-mail addresses: rvarela@iibce.edu.uy (R. Varela), irauschert@iibce.edu.uy (I. Rauschert), gromanelli@iibce.edu.uy (G. Romanelli), andresalberro@gmail.com (A. Alberro), jbenech@iibce.edu.uy, juanclaudio.benech@gmail.com (J.C. Benech).

https://doi.org/10.1016/j.bbrep.2021.100983
Received 11 August 2020; Received in revised form 4 February 2021; Accepted 8 March 2021

diabetic mice were stiffer than their control counterparts, and presented a disorganized actin cytoskeleton [29,30]. Additionally, it has been reported that diabetes induces differences in the F-actin spatial organization of the heart and skeletal muscles of the mouse [31].These results suggest that in DC, as well as in other pathologies like cancer [24,32,33], intrinsic mechanical property alterations at the cellular level are an important factor to be taken into account when attempting to explain -at least partially-the mechanical modifications observed at tissular level [28,29,31,33,34]. Moreover, intrinsic mechanical property alterations have been observed in other cell types such as vascular smooth muscle cells [35] or endothelial cells [21,22].

In DC, hyperglycemia and hyperlipidemia produce structural, biochemical and physiological alterations leading to major functional changes in the myocardium, which can lead to diastolic and systolic dysfunction and eventually to heart failure [36–38]. Different animal models have been used to study the effect of diabetes on the heart [31, 39,40]. However, using these models to study the specific effect of hyperglycemia and hyperlipidemia, separately or synergically, would be inappropriate [41,42]. Cell line cultures are a more suitable model to carry out these kinds of studies. A widely used model for the study of cardiac diseases is the H9c2 cell line [43]. This cell line has been found to maintain several of the physiological properties of cardiomyocytes [43–48]. Watkins and coworkers compared this cell line with neonatal primary cardiomyocytes and proved it is suitable for *in vitro* studies of cardiac diseases that generate hypertrophy [49]. It is a useful model for the study of the metabolic capacity of the heart [47], ischemia and reperfusion [50] and oxidative stress [51]. Previous studies have shown that high concentrations of G (22–33 mM) cause apoptotic cell death in adult cardiomyocytes and heart cells [41]. Palmitic acid at a concentration of 500 μM has been shown to induce myofibrils degeneration in adult cardiomyocytes [53] and apoptosis in neonatal cardiomyocytes [54]. In this work, to ascertain the morphophysiological changes that hyperglycemic and hyperlipidemic conditions can induce in cardiac cells we quantitatively analyzed the spatial changes induced by high G concentrations (25 and 33 mM) in the presence or absence of 500 μM palmitic acid. Furthermore, in the actin cytoskeleton of H9c2 cells, these changes were associated with changes in mechanical properties. The present study, to the best of our knowledge, is the first to generate elastic images of cardiac cells submitted to HHC and correlate nanomechanical changes detected at the cellular level with changes in the actin cytoskeleton.

2. Methods

2.1. Cell cultures

The study was conducted on an adherent H9c2 line of rat embryonic cardiomyocytes (ATCC, Manassas, VA, USA). Cells were grown on Dulbecco's Modified Eagle Medium (DMEM, Capricorn Scientific DMEM-LPXA) with 10% fetal bovine serum (Capricorn Scientific FBS-11A) at 37 °C with 5% CO_2, 100 U/mL of penicillin and 100 g/mL of streptomycin were added to prevent contamination. A concentration of 1×10^6 cells/mL was used divided into 10 cell culture petri dishes of 5 mL each. Different ampoules between 10 and 12 cell passages were used and cells were investigated at a confluency of 70% (maximum) [41].

Low G DMEM (G 5.5 mM) was used as the medium to grow control cells, and high G DMEM was used for two hyperglycemic conditions (G 25 mM and G 33 mM). As a hyperlipidemic medium, 500 μM of Palmitic Acid (PA, PO500 Sigma-Aldrich) in a complex with 1% bovine serum albumin (BSA, A3675, Sigma-Aldrich) was used. The PA/BSA complex was performed as detailed by several authors. Two solutions were prepared: Solution 1: Stock solution of 100 mM PA in 0.1 M NaOH at 70 °C with stirring. Solution 2: BSA solution at 10.5% m/v in distilled water at 55 °C and with stirring. To obtain the PA/BSA complex, 0.5 mL of solution 1 was mixed with 9.5 mL of solution 2, obtaining a stock solution of 5 mM PA/10% BSA. Subsequently, it was allowed to cool and filtered with a millipore membrane (0.22 μm) in a laminar flow chamber. The hyperglycemic (25 mM or 33 mM glucose) and hyperlipidemic medium was generated by adding 1/10 of the stock solution (5 mM PA/10% BSA), to obtain a final concentration of PA of 500 μM/1% BSA [42, 52–54].

2.2. Analysis of cell death induced by high glucose and lipid concentrations

2.2.1. Temporal analysis of cell death

A temporal analysis of cell death was performed in order to determine the optimal culture time in which the greatest number of cell death and morphological changes appear. The HHC at 12, 24, 36, 48, 60 and 72 h of culture was assessed. The same times to compare cell death in HHC were used in control conditions.

In all the cases the supernatant was collected and the cells were removed using trypsin/EDTA (0.05% in PBS 1 X) for 5 min at 37 °C. Subsequently, resuspended in DMEM low G and placed with the previously collected supernatant. After centrifugation at 800*g* for 5 min, the supernatant was discarded and the pellet was resuspended in PBS 1X. Cell viability was analyzed by incubating cells with propidium iodide (PI, 2 μg/mL, P4170, Sigma-Aldrich) for 5 min in the dark. Finally, 10 μL of the solution was loaded in a Neubauer chamber and the number of death and total cells were counted by Epifluorescence Microscopy (Olympus IX-81). 200 cells in each group were counted by two investigators independently in three independent experiments. Results were expressed as a percentage of cell death.

2.2.2. Analysis and quantitation of the optimal glucose conditions for the study of morphophysiological cell changes

To analyze the optimal G concentration for the study of morphophysiological cellular changes, the following conditions were evaluated: a) control (G 5.5 mM), b) G 5.5 mM + PA, c) G 25 mM, d) G 25 mM + PA, e) G 33 mM, f) HHC at 72 h of culture. In order to exclude a hyperosmolar effect, a control with 33 mM mannitol (M 33 mM) (M4125, Sigma-Aldrich) was included. Cell death quantification was performed following the same procedure as temporal analysis.

2.2.3. Analysis and quantitation of the type of cell death using the triple staining technique

Triple-staining technique was used to determine the type of cell death [55,56]. Stock solution (50 μL) contained a) 2.5 μL of PI (1 mg/mL), b) 7.5 μL of Hoechst 33,342 (1 mg/mL B2261, Sigma-Aldrich), c) 4.0 μL of Fluorescein diacetate (FDA, 1.5 mg/mL, F7378, Sigma-Aldrich), and d) 36 μL PBS 1X. Control and G 33 mM + PA cells (for subsequent studies, G 33 Mm + PA condition was called HHC) were grown during 72 h. The supernatant was collected and the cells were detached using trypsin/EDTA (0.05% in PBS 1x) for 5 min at 37 °C. Then the cells were centrifuged with the previously collected supernatant to preserve the death cells detached from the substrate. The pellets were resuspended in 50 μL PBS 1X, and 5 μL of stock solution was added in each case (6 min at room temperature in the dark). 10 μL of each sample was analyzed in a Confocal Laser Microscope (CLM, Olympus FV300). The cells were classified as vital, early apoptotic, late apoptotic and necrotic. The analysis was done in 100 cells, the assays were done per triplicate and by two investigators independently. Quantifications were represented as a percentage of the total cell death.

2.3. Cell morphophysiology analysis

2.3.1. Cell width and length quantitation in the different culture conditions

Optical microscopy (Nikon Diaphot 300) images were acquired to cell width and length measured using Micrometrics SE Premium software (NIH, USA). The analysis was performed at different times (0, 12, 24, 36, 48, 60, and 72 h) to the control and HHC cells. The analyses of the other conditions were made only at 72 h. An axis was drawn through

the two most distal points of each cell, and the distance between those two distal points was defined as the cell's length. In the middle of this segment, an axis was drawn perpendicular to the first one. The points where this axis intersects the cell's border were marked. The distance between those two points was defined as the cell's width. The analysis was done through independent experiments per triplicate by two independent collaborators, and 150 cells of each group were analyzed.

2.3.2. Analysis and quantitation of F-actin spatial organization

To study F-actin spatial organization images were acquired in the mid-focal plane at a resolution of 1024 × 1024, with a 40× objective, using CLM (Zeiss 800). Cells were cultivated on coverslips in two groups a) control and b) HHC. At 72 h, the cells were fixed in paraformaldehyde (PFA) 4% Triton X-100 0.2% (T8787, Sigma-Aldrich) for 10 min at room temperature. Cells were washed 3 times with PBS 1X and then incubated for 20 min with 6.6 μM phalloidin-rhodamine (R415, Thermofisher) at room temperature in the dark. Next, the cells were washed with PBS 1X for 3 times, and finally, were mounted with 50% glycerol-DAPI (1 μg/mL, D9542, Sigma-Aldrich).

To quantify the cell's length and width, an axis was drawn in the length of the cell (cell length) and an axis perpendicular to it in the middle of the cell length (cell width). A square of 10 μm × 10 μm was made in the axis intersection determining the central area. Two equal squares on the distal ends of the longitudinal axis were made to determine the peripheral area. The number of actin bundles and the distance between them were quantified in each square. As actin bundles are not always parallel to each other, a diagonal line was drawn from the upper left corner to the bottom right corner, and the distance between bundles was measured along that diagonal. Although most cells were affected by HHC, those with a length smaller than 60 μm were used to quantify. Three independent experiments were performed and a total of 150 cells were analyzed for each condition by two independent collaborators.

2.3.3. Analysis of cell stiffness maps obtained by atomic force microscopy

Stiffness, height and error images were obtained by atomic force microscopy (AFM, Bioscope Catalyst coupled with an Olympus IX-81). Height images contain data of the height changes necessary to keep deflection constant during scanning, and allow a high resolution reconstruction of the sample's topography. Error images contain data of where the height needed to be corrected, and thus contains better definition of the sample's structure. Bruker's QNM (Quantitative Nanomechanics) modulus was used, which allows the recorded data of the applied force and the deformation caused to be used to obtain quantitative values of Young's modulus (KPa) at each point. A DNP-10 (D) silicon nitride tip from the Brukercompany was used, with a radius of 20 nm (according to the manufacturer) and an elastic constant of 0.13 N/m (measured in liquid using the Thermal Tune tool). The maximum applied force varied between 5 nN and 8 nN. A total of 9 cells from each condition were analyzed. Image parameters were set to a scanning frequency of 0,125Hz, a resolution of 512 × 512 pixels and a scan size that allowed capturing an entire cell (between 100 μm and 150 μm). Once the entire cell was scanned the image was captured and scanning was halted, thus resulting in images that are not square.

The cells were cultivated in control or HHC for 72 h. The medium was removed and they were incubated in the dark with PI (1 μg/mL) for 5 min at room temperature to analyze only viable cells. The cells were washed with PBS 1X and placed in a 37 °C degree plate for analysis. Squares of 10 μm × 10 μm were made in the central and peripheral areas of the cell, similar for the quantitation of F-actin. These squares were defined in the error image to colocalize them in Young's modulus image and, thus, extract the modulus values for each pixel using the NanoScope Analysis software. Considering that each pixel of the image is a Young's modulus data, between 1200 and 2700 data points were used for each cell in each region. The variation in the number of data points is a consequence of the variations in scan size, as the scan rate was the same for all images. The extracted data were incorporated into the Graphpad Prism 8 software. Histograms were performed and a Gaussian fit was performed obtaining a stiffness value: mean ± SD.

2.3.4. Disruptive treatment of F-actin cytoskeleton

To study the relationship between cell stiffness and the F-actin cytoskeleton, H9c2 cells were incubated in control or HHC for 72 h and then treated with Cytochalasin D (Cyt. D, C8273 Sigma-Aldrich) in a 10 μM concentration for 30 min at 37 °C. After incubation, force curves were obtained in each case via the nanoindentation method. From each force curve, a value of the cell's Young's Modulus can be obtained; this value indicates the cell's stiffness.

2.3.5. Analysis of force curves obtained by atomic force microscopy

Force curves were obtained on live H9c2 cells in control or HHC after 72 h of incubation, with and without the Cyt. D treatment. The medium was removed and cells were incubated in the dark with PI (1 μg/mL) for 5 min at room temperature to analyze only viable cells. The cells were washed with PBS 1X and placed in a 37 °C degree plate for analysis. The same AFM was used with a DNP-10 (D) probe, with an elastic constant of 0.06 N/m according to the manufacturer's instructions. Force curves obtained in the central region of the cell at a frequency of 1 Hz. At least 250 force curves were obtained in each cell, and at least 1800 from each condition. Sneddon's model predicts that the quadratic coefficient of the applied force vs. indentation curve depends on the sample's Young's Modulus and the tip's geometry. From each force curve, a value of Young's Modulus was obtained from fitting the force curve with the Sneddon model [29,57]. Histograms were performed and a Gaussian fit was performed obtaining a stiffness value: mean ± SD.

2.4. Statistical analysis

A Shapiro-Wilk test was performed in all comparisons to verify the normality of the data. For those populations that did not meet the normality criteria, the Kruskal-Wallis non-parametric test was performed, and if there were differences between the groups, the Mann-Whitney-Wilcoxon test was performed. For those populations with n less than 30 data, a non-parametric test was used, without previously establishing normality. For those populations that were normal a Student's t-test was used, an ANOVA test was performed to compare all conditions.

All data were graphed using Graphpad Prism 8 software and statistical analyses were performed in R Studio software. Analysis of cell death and all the assays were done per triplicate. Values with $p < 0.05$ were considered as a significant difference.

3. Results

3.1. Analysis and quantitation of cell death

3.1.1. Effect of high glucose and lipid concentrations

Optical microscopy images of H9c2 cells (Fig. 1) were acquired from A) control (G 5.5 mM), B) G 5.5 mM + PA, C) G 25 mM, D) G 25 mM + PA, E) G 33 mM, F) HHC and G) M 33 mM conditions at 72 h in culture. The cells from the control group (Fig. 1A) had the characteristic fusiform morphology of the cell line. Cells cultured in M 33 mM (Fig. 1G) showed similar fusiform morphology and cell death with control ones, demonstrating that the observed cell death in G condition is not due to a hyperosmolar effect. Cell death quantitation of each condition at 72 h (Fig. 1H) did not show significant differences between the control (8.16% ± 0.25%), and M 33 mM (9.10% ± 0.85%) groups. However, with the addition of PA and with the increase in G concentration, cell death increased, evidencing a directly proportional relationship between G concentration and cell death. Both PA addition and G increase showed significant differences with respect to control (***Fig. 1H). Moreover, significant differences were found between the same G concentration with and without PA, demonstrating the influence of PA on

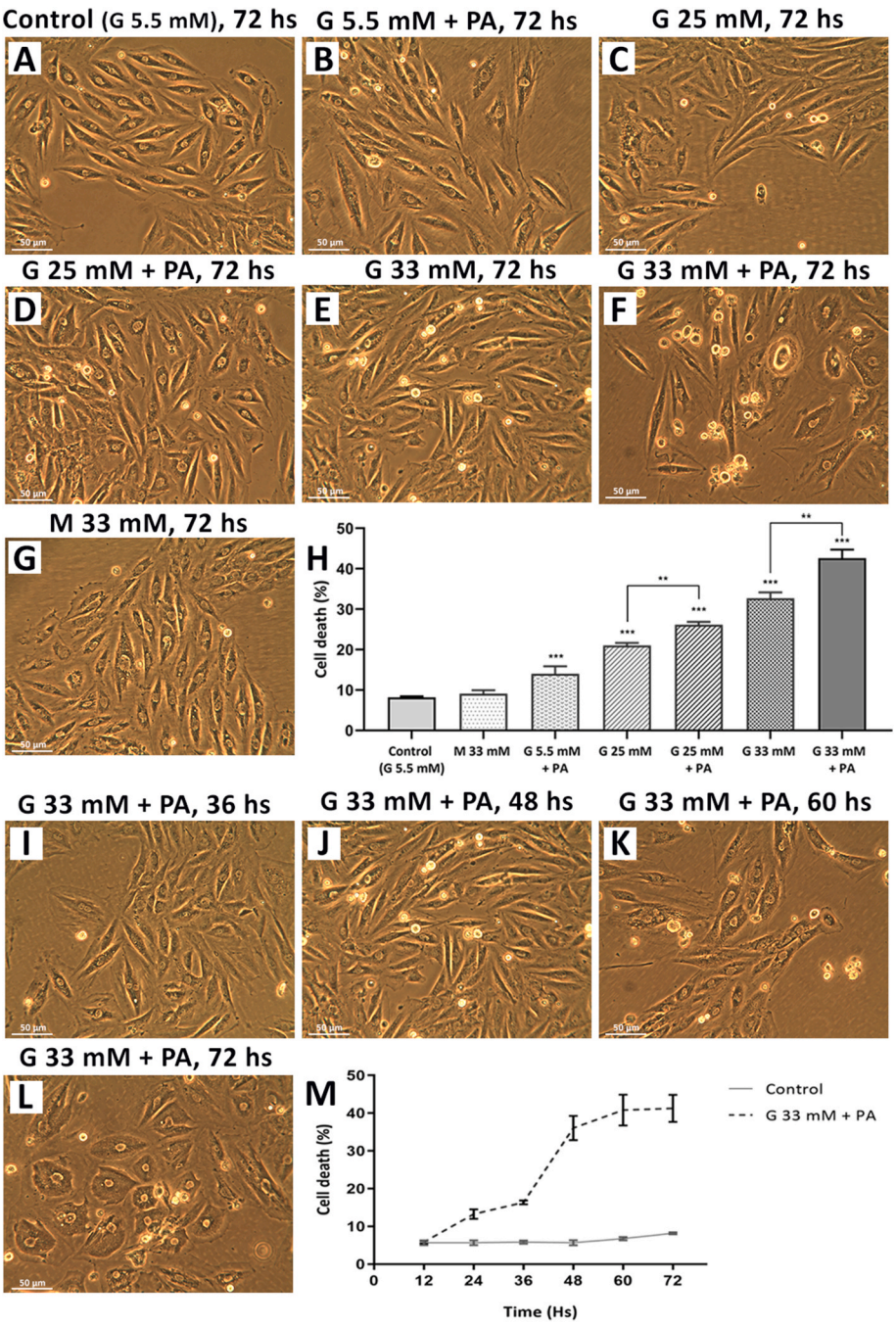

Fig. 1. Analysis and quantitation of cell death. Representative images obtained by light microscopy (10X) of the different cultures conditions of H9c2 being A) control (G 5.5 mM), B) G 5.5 mM + PA, C) G 25 mM, D) G 25 mM + PA, E) G 33 mM, F) G 33 mM + PA (HHC) and G) M 33 mM. H) Graph of cell death at 72 h of culture. Data expressed as a percentage of cell death for each condition. For the statistical analysis, a Kruskal-Wallis and Mann-Whitney tests were carried out, considering a $p < 0.05$ (***) as significant with respect to the control. Comparison of G 25 mM vs. G 25 mM + PA (**) and G 33 mM vs. HHC (**). **(I–M).** Cell death overtime in HHC. Representative images obtained by light microscopy (10X) of the H9c2 cultures every 24 h of incubation I) 36 h J) 48 h K) 60 h L) 72 h M) Graph of death cell as a function of time. Results obtained are expressed as a percentage of cell death with respect to the total number of cells. Three independent experiments were carried out for each condition, counting 200 cells in each group.

cell death (**Fig. 1H). Inclusion of BSA 1% without PA in the medium did not affect cell death (data not shown). Based on these results we defined and used the optimal condition for subsequent analyzes as HHC.

In order to determine the optimal cell culture time to carry out the subsequent studies, H9c2 cells were incubated under control conditions (Fig. 1A) for 72 h, and in HHC from 12 h to 72 h (Fig. 1I–L). In this way, cultures with differences of 12 h were obtained. The typical fusiform characteristic of this cell line was increasingly lost over time. At 72 h of cell culture, most of the cells had a completely different morphology compared with the control cells. Furthermore, it can be seen that there are more spaces between the cells, which would lead to less intercellular contact.

Quantitation of cell death for both conditions show a significant increase in the hours of culture elapsed in the HHC group compared with the control (Fig. 1M). At 72 h the percentage of cell death for the control reached a value of 8.16% ± 0.25% and for the HHC of 42.60% ± 3.60%.

3.1.2. *Type of cell death*

The triple staining technique was performed for the analysis of the type of cell death in control and HHC at 72 h of cell culture (Fig. 2). The images acquired by CLM show a representative vital cell, a cell in early apoptosis, and a cell in late apoptosis (Fig. 2A). In the fields visualized by the two independent researchers, no necrotic cells were observed.

Quantitation of early, late and total apoptosis indicates significant differences between control and HHC for all the stages of apoptosis (***Fig. 2B).

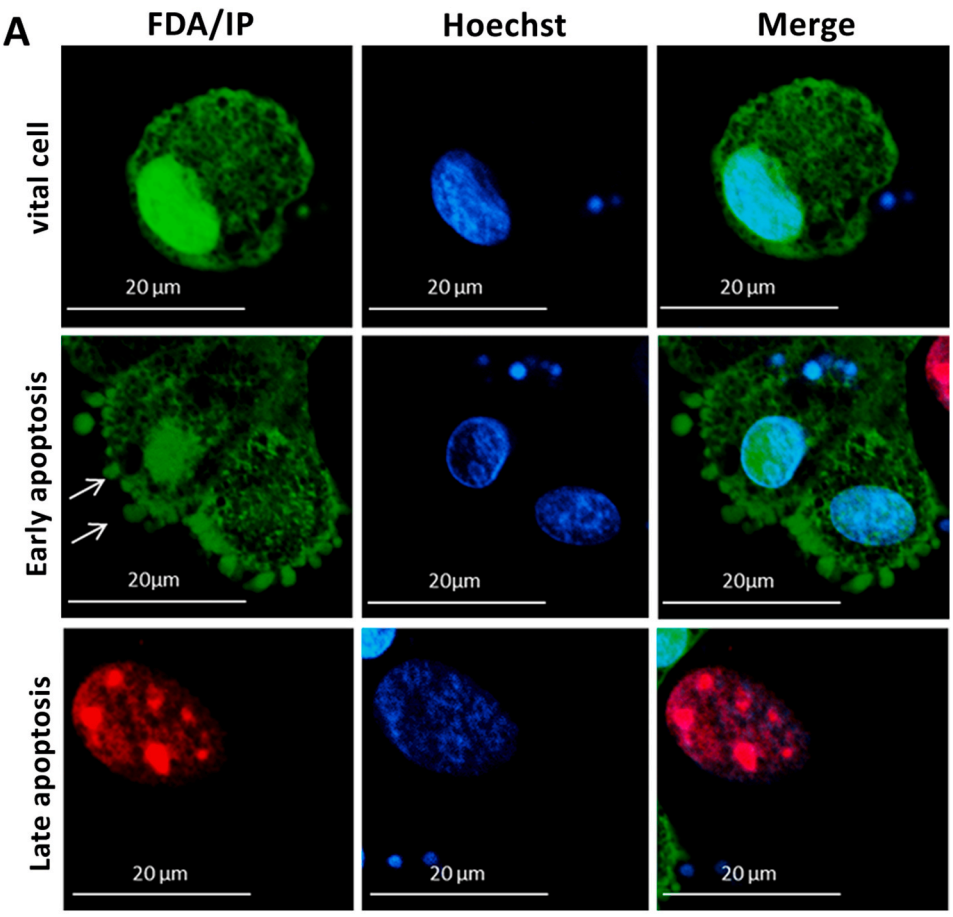

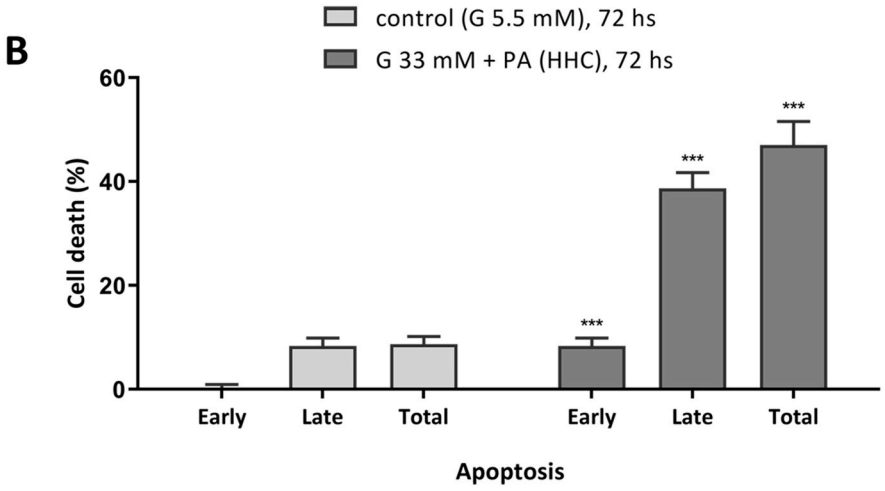

Fig. 2. Analysis and quantitation of apoptosis in cells cultured under control and HHC at 72 h A) Representative images of MLC (40X) of vital cells (top: green cell and normal blue nucleus), cells in early apoptosis (middle: green cell and blue nuclei with heterochromatic granules) and of cells in late apoptosis (bottom: red and blue nuclei with heterochromatic granules). The white arrows indicate the characteristic blebbing of early apoptosis. The red, green, and blue colors correspond to IP, FDA, and Hoechst respectively. B) Quantitation of early, late apoptotic and total cell death. Statistical analysis using the Kruskal-Wallis test was performed, $p < 0.05$ were considered significant (***). Three independent experiments were carried out for each condition, counting 100 cells in each group. (For interpretation of the references to color in this figure legend, the reader is referred to the Web version of this article.)

3.2. Morphophysiological analysis of cell changes induced by high glucose and lipid concentrations

3.2.1. Cell width and length quantitation in different experimental conditions

The results of the quantitation of cell length and width are shown in Fig. 3. Results of length quantitation show significant differences with respect to the control in G 25 mM and G 33 mM with and without PA (***). The differences in the length were greater with the increase in G concentration and with the addition of PA. The lowest length value being in HHC. There were also statistical differences between G 33 mM and HCC (*). Instead, in the width, significant differences were observed only under the G 33 mM and HHC (***). The greatest width values were measured in HHC.

3.2.2. Quantitation and analysis of actin cytoskeleton spatial organization

CLM images show cells stained with phalloidin-rhodamine (Fig. 4A–B). Control cells (Fig. 4A) exhibit actin bundles with homogeneous distribution throughout the entire cell. On the other hand, the actin bundles in HHC (Fig. 4B) have a very different organization. In this condition, most actin bundles are located mainly towards the cell periphery and are intertwined with each other.

Quantitation of the number of actin bundles in the central and distal zones of the cells showed significant differences (Fig. 4C). In the central zone, the number of actin bundles was significantly lower for cells grown in HHC than in controls. In contrast, the peripheral zone has a

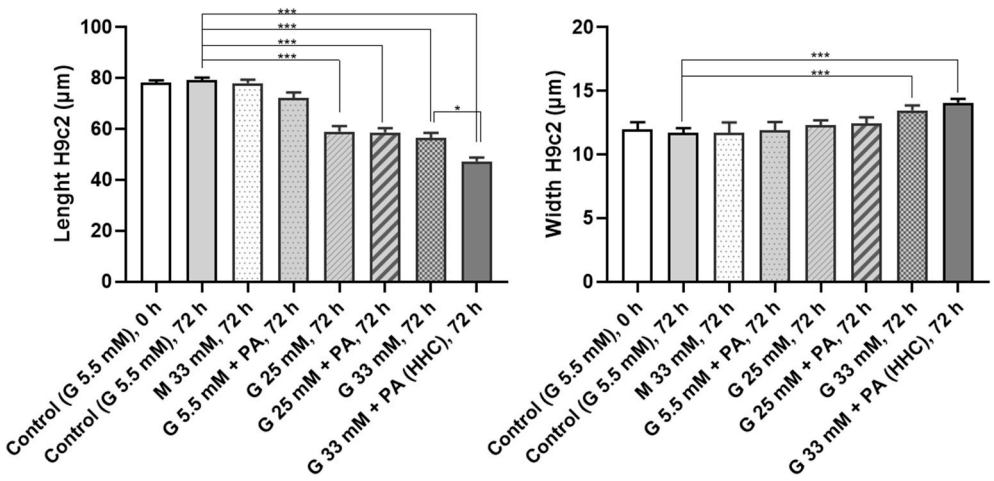

Fig. 3. Quantitation of cell length and width in the different experimental conditions. The figure shows the length and width of all experimental conditions (control (G 5.5 mM), M 33 mM, G 5.5 mM + PA, G 25 mM, G 25 mM + PA, G 33 mM and HHC). Three independent experiments were carried out for each condition, counting 200 cells in each group. Kruskal-Wallis was performed to compare all groups, and the Mann-Whitney test was performed to establish significant difference respect to the control group (***). A single asterisk (*) represent a significant difference between G 33 mM vs. HHC. Values with $p < 0.05$ were considered significant.

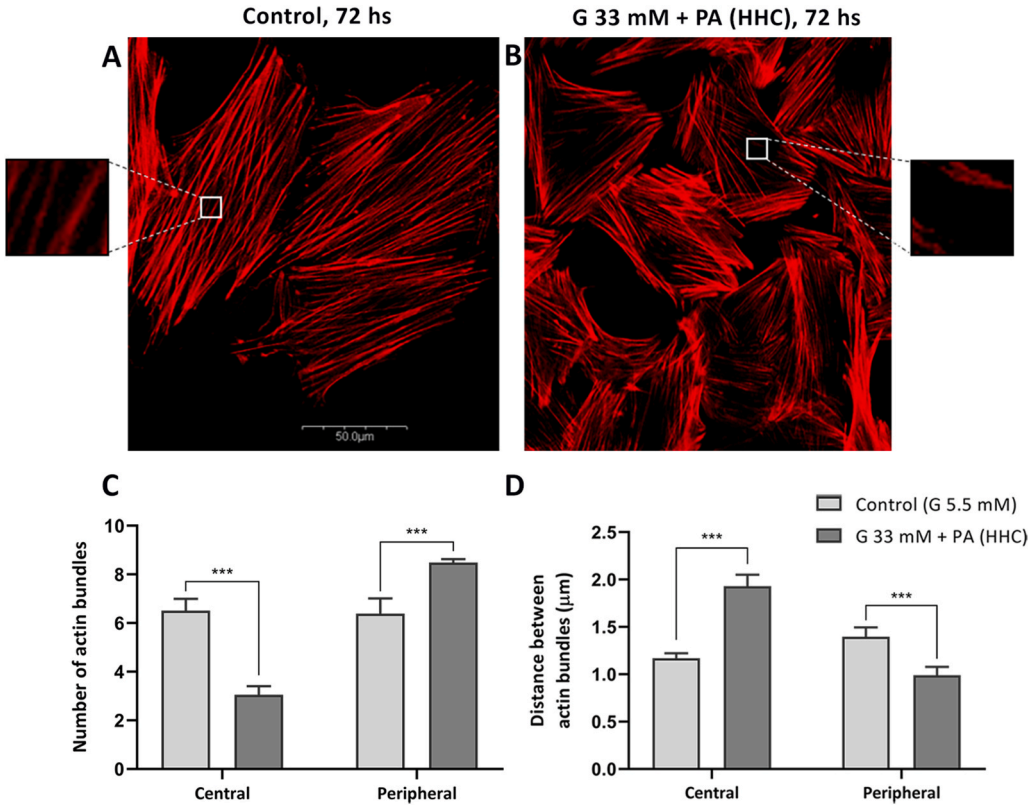

Fig. 4. Quantitation of actin spatial organization in control and HHC cardiac cells at 72 h. Representative images obtained by MLC of H9c2 cells stained with phalloidin-rhodamine (red). The 10 µm × 10 µm square is representatively enlarged. A) Control, B) HHC, C) Quantitation of the number of actin bundles of the central and peripheral zone, D) Quantitation of the distance of actin bundles of the central and peripheral zone. Three independent experiments were carried out for each condition, counting 150 cells in each group. Mann-Whitney test was performed, considering $p < 0.05$ (***) as significant. (For interpretation of the references to color in this figure legend, the reader is referred to the Web version of this article.)

significantly greater number of actin bundles in HHC compared to controls (Fig. 4C).

On the other hand, the quantitation of the distance between actin bundles also showed significant differences (Fig. 4D). In the central zone, the control cells showed a significantly shorter distance between the actin bundles than in the HHC. However, this comparison is inverted in the peripheral area. The actin bundles showed a significantly shorter distance in the HHC than in the controls.

3.2.3. *Analysis of cellular nanomechanics*

Representative AFM images of the living cells for both groups (control and HHC) at 72 h of incubation are shown in Fig. 5A. The error images show differences between the control and HHC cells. Control cells present fusiform characteristic shape and the HHC do not. Height images of control (n = 9) and HHC (n = 9) cells do not show significant differences (3.32 ± 0.31 and 4.00 ± 1.32 respectively). Young's modulus images show a cell stiffness map, allowing evaluating this nanomechanical property throughout the cell. Cells incubated in HHC were stiffer than control cells. Representative force-distance curves of control and HHC of central and peripheral zones are shown in Fig. 5B. Histograms obtained from the frequency of Young's modulus (cell stiffness) values allowed their quantitation (Fig. 5C). The dotted lines correspond to the Gaussian adjustments of each histogram. The values were extracted from the NanoScope Analysis software and were expressed in KPa. Both the central and distal areas of the cells were evaluated.

The mean and standard deviation values of the Gaussian adjustment of cell stiffness for each condition in the central and distal zones show significant differences (Table 1). Control cells have significant differences between the central and peripheral zones (*). They have a higher

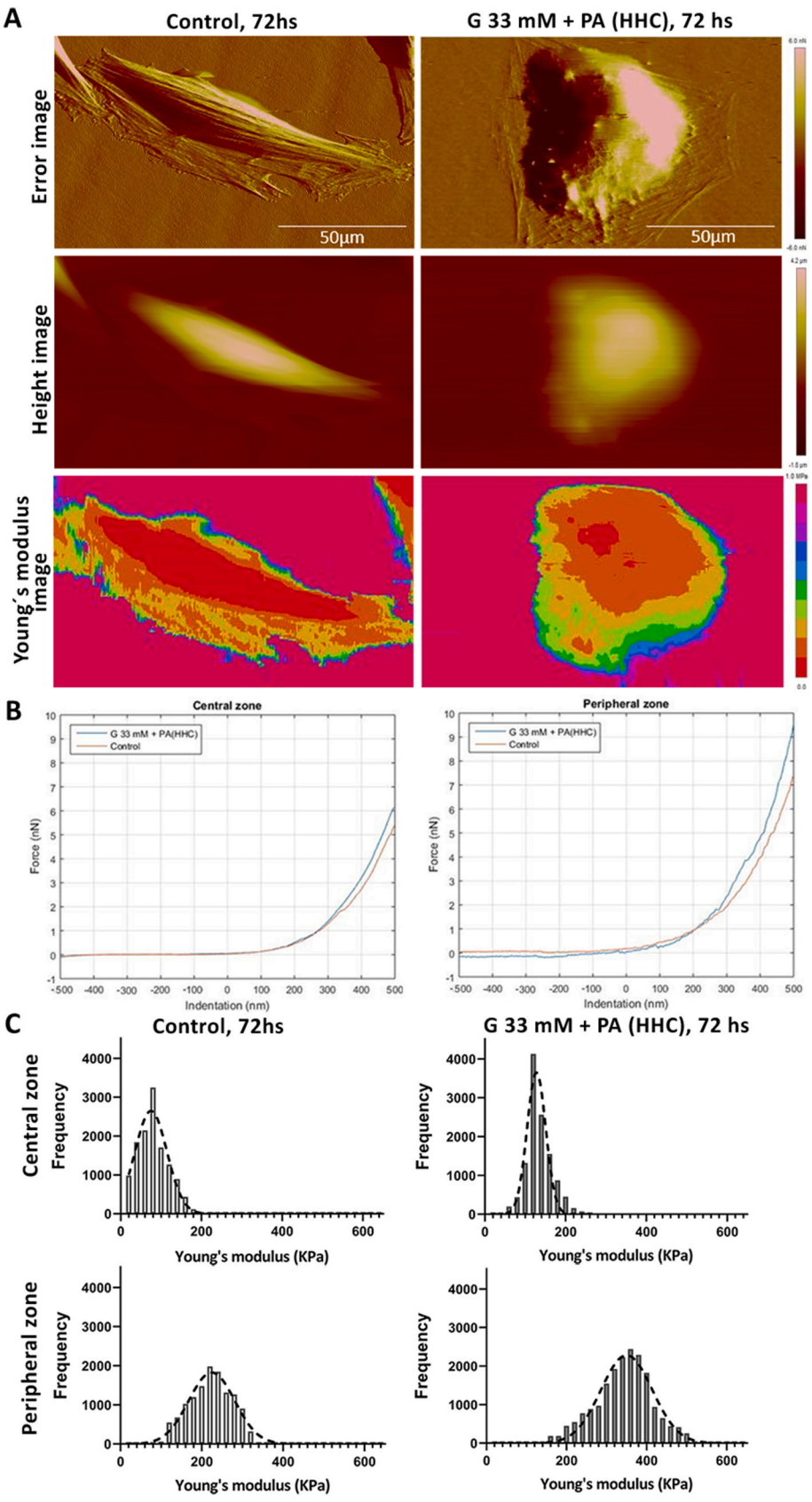

Fig. 5. Analysis and quantitation of cellular stiffness obtained by AFM at 72 h. A) Representative images of Error (peak force error), Height and Young's modulus images (cellular stiffness) of live cells obtained by AFM. The color scale in the stiffness images, with red representing values between 0 and 100 KPa, orange between 100 and 200 KPa, and so on. Nine cells from each group were analyzed. B) Representative force-distance curves of central and peripheral zones of control and HHC cells. C) Histograms show quantitation of cell stiffness obtained from Young's Modulus values. A total of 9 cells were analyzed for each group. The dotted lines correspond to the Gaussian fit of each histogram. (For interpretation of the references to color in this figure legend, the reader is referred to the Web version of this article.)

Table 1
Mean values of Young's modulus obtained from AFM. The mean values and standard deviations of the Gaussian fit from Young's modulus for each condition in the central and peripheral zones of the cells are shown. A total of nine cells were analyzed for each group. ANOVA test was performed to compare all conditions, and Student's t-test. To compare central and peripheral zones. $p < 0.05$ was considered significant. Central vs. peripheral zones of the control group (*), peripheral control vs. peripheral HHC zones (**), central vs. peripheral zones of HHC (***).

	Central zone (kPa)	Periphery zone (kPa)
Control, 72 hs	78.90 ± 36.40	222.20 ± 57.40 *
G 33 mM + PA, 72 hs	122.70 ± 26.10***	358.8 ± 64.00 **/***

Young's modulus values in the peripheral than in the central zone. Also, peripheral and central zones of HHC have statistical differences (**), being the peripheral zone stiffer than the central zone too. The peripheral zone of both groups also has differences. The control peripheral zone has statistically lower Young's modulus values than HHC (***). Finally, no statistical differences were found between the central zones of both groups.

3.2.4. Young's modulus and actin cytoskeleton

The biomechanical properties of animal cells are determined primarily by their cytoskeleton. As a way of evaluating the contribution of the actin cytoskeleton to the value of Young's modulus in H9c2 cells, we used the nanoindentation method [29] in the presence or absence 10 μM of Cyt. D (***Fig. 6). The treatment of control cells with the mentioned drug produced a significant decrease in Young's modulus from 89.3 ± 23.6 kPa to 47.5 ± 21.9 kPa (47%). In the HHC, 10 μM Cyt. D treatment also significantly reduced the value of Young's modulus from 117.9 ± 26.4 kPa (without the drug) to 36.4 ± 21.1 kPa (in the presence of the drug). Therefore, a reduction of 69% observed in Young's modulus (***Fig. 6).

4. Discussion

Hyperglycemia and hyperlipidemia are known to play an important role in the development of DC, independent of other factors [42,58,59]. In this paper, the H9c2 cell line was used to study morphological changes induced by HHC in heart cells. Obtained results showed that HHC induced apoptotic cell death, changes in cell shape, changes in the spatial distribution of actin cytoskeleton, and the stiffening of the elasticity images of living heart cells obtained by AFM. The results suggest the existence of a relationship between the spatial modification of the actin cytoskeleton and the stiffening of the cardiac cell that can help to understand the complicated process behind the pathophysiology of DC.

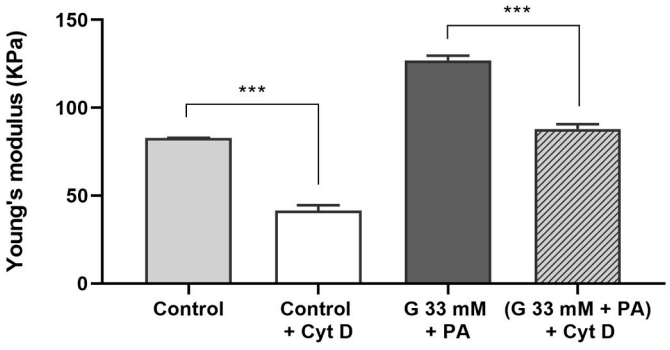

Fig. 6. Effect of Cytochalasin D on cell stiffness in control and HHC H9c2 cells. A total of nine cells of each condition were analyzed. Student's t-test was applied, considering $p < 0.05$ (***) as significant.

4.1. Analysis of cell death and morphological changes

Previous studies have shown apoptotic cell death in adult cardiomyocytes and cardiac cells due to high G concentrations [41] and the deleterious effect that high concentrations of G and PA have on adult cardiomyocyte myofibrils [53]. Accordingly, in this work, we also observed an increase in cell death with increased G concentration [41] and 500 μM PA concentration [54]. With a concentration of G 25 mM, cell death increased 2.6 fold when compared to the control. With the aforementioned G concentration, the increase in cell death was significantly higher (3.2 times respect to control) by the addition of 500 μM of PA (Fig. 1). With a concentration of G 33 mM in the incubation medium, cell death increased 4.0 fold compared to the control. With the last G concentration, the increase in cell death was also significantly higher (5.2 times respect to control) by the addition of 500 μM of PA (Fig. 1). These results show the synergic effect of G and PA. However, cell death showed no significant differences when compared to the control by inclusion in the medium of M 33 mM. This result suggests that the increase in cell death is not due to a hyperosmotic effect due to high G concentration.

In addition to an increase in cell death, our study also detected changes in cellular morphology. Our results suggest that with G 25 mM and 25 mM + PA only cell length had a significant variation with respect to the control. However, in G 33 mM and HHC the changes were significant in cell length and width (Fig. 3). As previously expressed in results, no significant differences in height with respect to control were detected in HHC cells (Fig. 5A, Height image). Comparing the condition HHC with control at 72 h, the cell length decreased 1.7 times and the cell width increased 1.2 times. These results are consistent with a study on streptozotocin (STZ) induced Type 1 DM mice in which changes in the morphology of diabetic cardiomyocytes were observed [60]. It can also be noted that the variations between control and treatment with M 33 mM were not significant, which reaffirms again that the changes induced by the medium HHC are not due to a hyperosmotic effect (Fig. 3).

Hyperglycemia and hyperlipidemia produce elevated levels of reactive oxygen species (ROS) that generate changes in the morphology of cardiomyocytes and H9c2 and generate high levels of cell death by apoptosis [41,51,61,62]. It has also been reported that ROS induced apoptosis by activation of caspase-3 [63], in cardiomyocytes of STZ-induced diabetic rat and mouse models [41,64], and *in vitro* models like H9c2 cells [41].

It is known that the high concentration of G increases the absorption and oxidation of free fatty acid generating an increase in cellular apoptosis [28,65]. All of these observations are consistent with our results where the cell death type analysis showed only apoptotic death with significantly greater differences for the HHC group between early and late apoptosis (Fig. 2 B).

4.2. Analysis of F actin spatial organization and cell nanomechanics

Recently, it has been reported that the spatial organization of F-actin is modified in the myocardium of type 1 DM mice [31]. In the present study, conducted with H9c2 cells, we observed a marked displacement of the F-actin cytoskeleton toward the cell periphery in the HHC when compared to the control condition. It is difficult to accurately measure and say whether the fluorescence signal corresponds to individual actin filaments or bundles of actin. Then we prefer to refer to these structures as bundles of actin (which also includes individual filaments). The number of actin bundles in the distal area was 2.83 times higher and the distance between them was 1.9 times smaller for the HHC at 72 h of incubation when compared to the control condition (Fig. 4). This same behavior of actin cytoskeleton has been observed in vascular cells of the smooth musculature [35] and in H9c2 cells when these cells were treated with a strong inductor of hypertrophy such as endothelin [49]. It is also known that glucolipotoxicity generates significant alterations in

the actin cytoskeleton [53,66]. Modifications in the cell cytoskeleton of neonatal cardiomyocytes induced by liposaccharides and detected by AFM have also been reported [67]. Cell mechanics can provide information on the cell physiological or pathological state processes like aging [68], differentiation [69,70] or disease [71]. Pathological changes in mechanical properties start at the cellular scale and then spread to higher levels of organization such as tissues and organs. Therefore, the investigation of the mechanics of the single diseased cells may provide deeper insights into pathological processes [33]. The biomechanical properties of animal cells are mainly determined by their cytoskeleton [72–74]. In isolated adult cardiomyocytes, Wu and colleagues showed that Young's modulus value, determined by the nanoindentation method, was around 80% actin dependent [26]. These authors showed the decrease of Young's modulus in cardiomyocytes when the cells were treated with Cyt. D (an F-actin-disrupting agent). In the absence of Cyt. D, the stiffness was approximately 30 kPa and approximately 5 kPa in the presence of the drug [26]. According to our results, in H9c2 cells, Young's modulus was also affected by the treatment with Cyt. D. Since Cyt. D treatment was only for 30 min, most likely the effect observed on Young's decreased module (47% in control and 69% in HHC) was due to a direct effect on the disruption of actin cytoskeleton (Fig. 6).

Our study is the first to obtain complete comparative elasticity maps of heart cells incubated under control or HHC. Elasticity maps reveal the drastic change that the HHC induces in the elasticity of heart cells. Cellular elasticity is one of its physiological properties.

Analysis of elasticity maps showed that the rigidity of cells incubated in the HHC was greater than those incubated in the control condition, being 1.54 fold greater in the central region and 1.63 fold greater in the distal region (Fig. 5C and Table 1). These results are consistent with previous results observed by other authors [29,42]. Benech and colleagues demonstrated an increase in the value of Young's modulus, when working with adult cardiomyocytes isolated from type 1 DM mice, presenting controls cardiomyocytes a stiffness of 43 KPa ±7 KPa and diabetic cardiomyocytes 91 KPa ±14 KPa [29,30]. Michaelson and colleagues also reported an increase in cellular stiffness in isolated neonatal cardiomyocytes incubated under conditions of hyperglycemia (30.5 mM) or hyperlipidemia (500 μM PA). In both conditions, the authors report that they did not observe any modifications in the actin cytoskeleton. It is important to note that the aforementioned authors did not conduct the study in a hyperglycemic and hyperlipidemic medium as in our case (HHC). Also, the incubation time of the cells they used was shorter (24 h). Perhaps, to clearly observe the modifications of the actin cytoskeleton, a joint action of hyperglycemia and hyperlipidemia would be necessary for a longer period.

Like the results reported by Shroff and colleagues in cultured rat atrial myocytes, in our study, we also found differences in the elasticity of H9c2 cells between the central and the peripheral region [75]. The peripheral region was stiffer in both the control condition and the HHC (Fig. 5 and Table 1).

Since Young's modulus in H9c2 cells showed to be most likely actin dependent and that the HHC medium promoted a reordering of the actin cytoskeleton, our results suggest a correlation between the reordering of the actin cytoskeleton and the modulus of elasticity. This suggestion is based on the fact that the reordering of the actin cytoskeleton was quantified and the number and distance of actin bundles were not the same in the control as under HHC (Fig. 4). Cells incubated in HHC with the reordered actin cytoskeleton were stiffer than those incubated in the control condition (Fig. 5 and Table 1). The peripheral zone of the HHC (where the number of actin bundles was higher and the distance between them smaller) was the region of greatest stiffness (Figs. 4 and 5 and Table 1).

5. Conclusions

The results obtained *in vitro* with the H9c2 rat cardiac cell model suggest that HHC in addition to inducing apoptotic cell death can modify the spatial distribution of actin cytoskeleton at the cellular level. This results in the modification of the properties of cellular biomechanics that probably would affect biomechanics at the organ level (heart). Thus, our study showed that HHC promotes morphophysiological changes in rat cardiac cells confirming that gluco-and lipotoxicity may play a central role in the development of DC.

Author contributions

Rocío Varela: performed experiments, collected and performed the data analyses and contributed to the discussion. Inés Rauschert: performed experiments, collected and performed the data analyses and contributed to the discussion. Gerardo Romanelli: performed the data analyses, contributed to the discussion and with paper writing. Andrés Alberro: performed experiments, collected and performed the data analyses. Juan C. Benech: conceived the study, obtained research funding, wrote the paper and approved the final version of the manuscript. Is the guarantor of this work and, as such, had full access to all the data in the study and takes responsibility for the integrity of the data and the accuracy of the data analysis. Is the corresponding author.

Funding

This work was supported by ANII (grant number FCE_1_2017_136.045), Uruguay and partially by PEDECIBA, Uruguay.

CRediT authorship contribution statement

Rocío Varela: Conceptualization, Methodology, Investigation, Formal analysis. **Inés Rauschert:** Conceptualization, Methodology, Investigation, Data curation. **Gerardo Romanelli:** Conceptualization, Formal analysis, Data curation, Visualization, Writing – original draft, preparation. **Andrés Alberro:** Investigation, Formal analysis, Visualization. **Juan C. Benech:** Conceptualization, Writing – review & editing, Supervision, Project administration, Funding acquisition.

Declaration of competing interest

The authors declare that they have no known competing financial interests or personal relationships that could have appeared to influence the work reported in this paper.

Acknowledgments

We thank Drs. Gonzalo Ferreira, Facultad de Medicina, UdelaR, Aldo Calliari, Facultad de Veterinaria, UdelaR and María Vittoria Di Tomaso, IIBCE, for their constructive comments and suggestions on the manuscript.

References

[1] L. Guariguata, D.R. Whiting, I. Hambleton, J. Beagley, U. Linnenkamp, J.E. Shaw, Global estimates of diabetes prevalence for 2013 and projections for 2035, Diabetes Res. Clin. Pract. 103 (2014) 137–149, https://doi.org/10.1016/j.diabres.2013.11.002.

[2] P. Zimmet, K.G. Alberti, D.J. Magliano, P.H. Bennett, Diabetes mellitus statistics on prevalence and mortality: facts and fallacies, Nat. Rev. Endocrinol. 12 (2016) 616–622, https://doi.org/10.1038/nrendo.2016.105.

[3] International Diabetes Federation, IFD diabetes atlas. https://Www.Diabetesatlas.Org/En/, 2019. (Accessed 31 July 2020).

[4] I. Gil-ortega, J. Carlos, Miocardiopatía diabética 127 (2006) 584–594, https://doi.org/10.1157/13094003.

[5] D. Mozaffarian, J.E. Benjamin, S.A. Go, K.D. Arnett, J.M. Blaha, M. Cushman, S. de Ferranti, J.-P. Després, J.H. Fullerton, J.V. Howard, D.M. Huffman, E.S. Judd, M. B. Kissela, T.D. Lackland, H.J. Lichtman, D.L. Lisabeth, S. Liu, H.R. Mackey, B. D. Matchar, K.D. McGuire, R.E. Mohler, S.C. Moy, P. Muntner, E.M. Mussolino, K. Nasir, W.R. Neumar, G. Nichol, L. Palaniappan, K.D. Pandey, J.M. Reeves, J. C. Rodriguez, D.P. Sorlie, J. Stein, A. Towfighi, N.T. Turan, S.S. Virani, Z.J. Willey, D. Woo, W.R. Yeh, B.M. Turner, Heart disease and stroke statistics–2015 update: a

report from the American Heart Association, Circulation 131 (2015) 29–322, https://doi.org/10.1161/CIR.0000000000000152.
[6] S. Rubler, J. Dlugash, Y.Z. Yuceoglu, T. Kumral, A.W. Branwood, A. Grishman, New type of cardiomyopathy associated with diabetic glomerulosclerosis, Am. J. Cardiol. 30 (1972) 595–602, https://doi.org/10.1016/0002-9149(72)90595-4.
[7] G. Jia, A. Whaley-Connell, J.R. Sowers, Diabetic cardiomyopathy: a hyperglycaemia- and insulin-resistance-induced heart disease, Diabetologia 61 (2018) 21–28, https://doi.org/10.1007/s00125-017-4390-4.
[8] M. Lehrke, N. Marx, Diabetes mellitus and heart failure, Am. J. Cardiol. 120 (2017) S37–S47, https://doi.org/10.1016/j.amjcard.2017.05.014.
[9] K.S. Spector, Diabetic cardiomyopathy, Clin. Cardiol. 21 (1998) 885–887, https://doi.org/10.1002/clc.4960211205.
[10] D.N. Tziakas, G.K. Chalikias, J.C. Kaski, Epidemiology of the diabetic heart, Coron. Artery Dis. 16 (1) (2005) S3–S10, https://doi.org/10.1097/00019501-200511001-00002.
[11] S.W. Zarich, B.E. Arbuckle, L.R. Cohen, M. Roberts, R.W. Nesto, Diastolic abnormalities in young asymptomatic diabetic patients assessed by pulsed Doppler echocardiography, J. Am. Coll. Cardiol. 12 (1988) 114–120, https://doi.org/10.1016/0735-1097(88)90364-6.
[12] A. Jain, G. Avendano, S. Dharamsey, A. Dasmahapatra, R. Agarwal, A. Reddi, T. Regan, Left ventricular diastolic function in hypertension and role of plasma glucose and insulin, Circulation 93 (1996) 1396–1402, https://doi.org/10.1161/01.CIR.93.7.1396.
[13] M. Diamant, H.J. Lamb, Y. Groeneveld, E.L. Endert, J.W.A. Smit, J.J. Bax, J. A. Romijn, A. de Roos, J.K. Radder, Diastolic dysfunction is associatedwith altered myocardial metabolism inasymptomatic normotensive patientswith well-controlled type 2 diabetes mellitus, J. Am. Coll. Cardiol. 42 (2003) 328–335, https://doi.org/10.1016/S0735-1097(03)00625-9.
[14] K.H. van Hoeven, S.M. Factor, A comparison of the pathological spectrum of hypertensive, diabetic, and hypertensive-diabetic heart disease, Circulation 82 (1990) 848–855, https://doi.org/10.1161/01.cir.82.3.848.
[15] T.J. Berg, O. Snorgaard, J. Faber, P.A. Torjesen, P. Hildebrandt, J. Mehlsen, K. F. Hanssen, Serum levels of advanced glycation end products are associated with left ventricular diastolic function in patients with type 1 diabetes, Diabetes Care 22 (1999) 1186–1190, https://doi.org/10.2337/diacare.22.7.1186.
[16] Z.Y. Fang, J.B. Prins, T.H. Marwick, Diabetic cardiomyopathy: evidence, mechanisms, and therapeutic implications, Endocr. Rev. 25 (2004) 543–567, https://doi.org/10.1210/er.2003-0012.
[17] J.A. Heier, D.J. Dickinson, A. V Kwiatkowski, Measuring protein binding to F-actin by Co-sedimentation, JoVE (2017), https://doi.org/10.3791/55613.
[18] T.D. Pollard, Actin and actin-binding proteins, Cold Spring Harbor Perspectives in Biology 8 (2016) a018226, https://doi.org/10.1101/cshperspect.a018226.
[19] N.L. Sehgel, Y. Zhu, Z. Sun, J.P. Trzeciakowski, Z. Hong, W.C. Hunter, D.E. Vatner, G.A. Meininger, S.F. Vatner, Increased vascular smooth muscle cell stiffness: a novel mechanism for aortic stiffness in hypertension, Am. J. Physiol. Heart Circ. Physiol. 305 (2013) H1281–H1287, https://doi.org/10.1152/ajpheart.00232.2013.
[20] Y. Zhu, H. Qiu, J.P. Trzeciakowski, Z. Sun, Z. Li, Z. Hong, M.A. Hill, W.C. Hunter, D.E. Vatner, S.F. Vatner, G.A. Meininger, Temporal analysis of vascular smooth muscle cell elasticity and adhesion reveals oscillation waveforms that differ with aging, Aging Cell 11 (2012) 741–750, https://doi.org/10.1111/j.1474-9726.2012.00840.x.
[21] J. Fels, P. Jeggle, I. Liashkovich, W. Peters, H. Oberleithner, Nanomechanics of vascular endothelium, Cell Tissue Res. 355 (2014) 727–737, https://doi.org/10.1007/s00441-014-1853-5.
[22] K.B. Grimm, H. Oberleithner, J. Fels, Fixed endothelial cells exhibit physiologically relevant nanomechanics of the cortical actin web, Nanotechnology 25 (2014) 215101, https://doi.org/10.1088/0957-4484/25/21/215101.
[23] K. Kusche-Vihrog, P. Jeggle, H. Oberleithner, The role of ENaC in vascular endothelium, Pflueg. Arch. Eur. J. Physiol. 466 (2014) 851–859, https://doi.org/10.1007/s00424-013-1356-3.
[24] I. Rauschert, F. Aldunate, J. Preussner, M. Arocena-Sutz, V. Peraza, M. Looso, J. C. Benech, R. Agrelo, Promoter hypermethylation as a mechanism for Lamin A/C silencing in a subset of neuroblastoma cells, PloS One 12 (2017), e0175953, https://doi.org/10.1371/journal.pone.0175953 e0175953.
[25] U.G. Hofmann, C. Rotsch, W.J. Parak, M. Radmacher, Investigating the cytoskeleton of chicken cardiocytes with the atomic force microscope, J. Struct. Biol. 119 (1997) 84–91, https://doi.org/10.1006/jsbi.1997.3868.
[26] X. Wu, Z. Sun, A. Foskett, J.P. Trzeciakowski, G.A. Meininger, M. Muthuchamy, Cardiomyocyte contractile status is associated with differences in fibronectin and integrin interactions, Am. J. Physiol. Heart Circ. Physiol. 298 (2010) H2071–H2081, https://doi.org/10.1152/ajpheart.01156.2009.
[27] D. Borin, I. Pecorari, B. Pena, O. Sbaizero, Novel insights into cardiomyocytes provided by atomic force microscopy, Semin. Cell Dev. Biol. 73 (2018) 4–12, https://doi.org/10.1016/j.semcdb.2017.07.003.
[28] G. Romanelli, R. Varela, I. Rauschert, C. Espasandín, J.C. Benech, New Aproaches to the Morphophysiological Study of Cardiomyocytes with Clinical Relevance, 2019. New York.
[29] J.C. Benech, N. Benech, A.I. Zambrana, I. Rauschert, V. Bervejillo, N. Oddone, J. P. Damián, Diabetes increases stiffness of live cardiomyocytes measured by atomic force microscopy nanoindentation, Am. J. Physiol. Cell Physiol. 307 (2014) C910–C919. http://ajpcell.physiology.org/content/307/10/C910.abstract.
[30] J.C. Benech, N. Benech, A.I. Zambrana, I. Rauschert, V. Bervejillo, N. Oddone, Intrinsic nanomechanical changes in live diabetic cardiomyocytes, Cardiovascular Regenerative Medicine 2 (2015) 1–8, https://doi.org/10.14800/crm.893.
[31] G. Romanelli, R. Varela, J.C. Benech, Diabetes induces differences in the F-actin spatial organization of striated muscles, Cytoskeleton (2020) 1–12, https://doi.org/10.1002/cm.21600.
[32] M. Lekka, P. Laidler, G. Dorota, J. Lekki, Z. Stachura, A.Z. Hrynkiewicz, Elasticity of normal and cancerous human bladder cells studied by scanning force microscopy, Eur. Biophys. J. 28 (1999) 312–316, https://doi.org/10.1007/s002490050213.
[33] C. Rianna, M. Radmacher, Cell mechanics as a marker for diseases: biomedical applications of AFM, AIP Conference Proceedings 1760 (2016), https://doi.org/10.1063/1.4960276.
[34] G.A. Meininger, The central importance of the cytoskeleton for increased cell stiffness in cardiovascular disease. Focus on "Diabetes increases stiffness of live cardiomyocytes measured by atomic force microscopy nanoindentation, Am. J. Physiol. Cell Physiol. 307 (2014) C908–C909, https://doi.org/10.1152/ajpcell.00279.2014.
[35] H. Qiu, Y. Zhu, Z. Sun, J.P. Trzeciakowski, M. Gansner, C. Depre, R.R.G. Resuello, F.F. Natividad, W.C. Hunter, G.M. Genin, E.L. Elson, D.E. Vatner, G.A. Meininger, S.F. Vatner, Short communication: vascular smooth muscle cell stiffness as a mechanism for increased aortic stiffness with aging, Circ. Res. 107 (2010) 615–619, https://doi.org/10.1161/CIRCRESAHA.110.221846.
[36] S. Arvan, K. Singal, R. Knapp, A. Vagnucci, Subclinical left ventricular abnormalities in young diabetics, Chest 93 (1988) 1031–1034, https://doi.org/10.1378/chest.93.5.1031.
[37] M. Galderisi, K.M. Anderson, P.W. Wilson, D. Levy, Echocardiographic evidence for the existence of a distinct diabetic cardiomyopathy (the Framingham Heart Study), Am. J. Cardiol. 68 (1991) 85–89, https://doi.org/10.1016/0002-9149(91)90716-x.
[38] P.H. Stone, J.E. Muller, T. Hartwell, B.J. York, J.D. Rutherford, C.B. Parker, Z. G. Turi, H.W. Strauss, J.T. Willerson, T. Robertson, E. Braunwald, A.S. Jaffe, The effect of diabetes mellitus on prognosis and serial left ventricular function after acute myocardial infarction: contribution of both coronary disease and diastolic left ventricular dysfunction to the adverse prognosis, J. Am. Coll. Cardiol. 14 (1989) 49–57, https://doi.org/10.1016/0735-1097(89)90053-3.
[39] A.J.F. King, The use of animal models in diabetes research, Br. J. Pharmacol. 166 (2012) 877–894, https://doi.org/10.1111/j.1476-5381.2012.01911.x.
[40] S. Boudina, E.D. Abel, Diabetic cardiomyopathy revisited, Circulation 115 (2007) 3213–3223. http://circ.ahajournals.org/content/115/25/3213.abstract.
[41] L. Cai, W. Li, G. Wang, L. Guo, Y. Jiang, Y.J. Kang, Hyperglycemia-induced apoptosis in mouse myocardium, Diabetes 51 (2002) 1938–1948, https://doi.org/10.2337/diabetes.51.6.1938.
[42] J. Michaelson, V. Hariharan, H. Huang, Hyperglycemic and hyperlipidemic conditions alter cardiac cell biomechanical properties, Biophys. J. 106 (2014) 2322–2329, https://doi.org/10.1016/j.bpj.2014.04.040.
[43] B.W. Kimes, B.L. Brandt, Properties of a clonal muscle cell line from rat heart, Exp. Cell Res. 98 (1976) 367–381, https://doi.org/10.1016/0014-4827(76)90447-X.
[44] J. Hescheler, R. Meyer, S. Plant, D. Krautwurst, W. Rosenthal, G. Schultz, Morphological, biochemical, and electrophysiological characterization of a clonal cell (H9c2) line from rat heart, Circ. Res. 69 (1991) 1476–1486. http://circres.ahajournals.org/content/69/6/1476.abstract.
[45] L. Cai, Y.J. Kang, Cell death and diabetic cardiomyopathy, Cardiovasc. Toxicol. 3 (2003) 219–228, https://doi.org/10.1385/CT:3:3:219.
[46] C. Ménard, S. Pupier, D. Mornet, M. Kitzmann, J. Nargeot, P. Lory, Modulation of L-type calcium channel expression during retinoic acid-induced differentiation of H9C2 cardiac cells, J. Biol. Chem. 274 (1999) 29063–29070, https://doi.org/10.1074/jbc.274.41.29063.
[47] B.N.M. Zordoky, A.O.S. El-Kadi, H9c2 cell line is a valuable in vitro model to study the drug metabolizing enzymes in the heart, J. Pharmacol. Toxicol. Methods 56 (2007) 317–322, https://doi.org/10.1016/j.vascn.2007.06.001.
[48] M. Park, A. Sabetski, Y. Kwan Chan, S. Turdi, G. Sweeney, Palmitate induces ER stress and autophagy in H9c2 cells: implications for apoptosis and adiponectin resistance, J. Cell. Physiol. 230 (2015) 630–639, https://doi.org/10.1002/jcp.24781.
[49] S.J. Watkins, G.M. Borthwick, H.M. Arthur, The H9C2 cell line and primary neonatal cardiomyocyte cells show similar hypertrophic responses in vitro, in Vitro Cellular & Developmental Biology, Animal 47 (2011) 125–131, https://doi.org/10.1007/s11626-010-9368-1.
[50] H. Han, H. Long, H. Wang, J. Wang, Y. Zhang, Z. Wang, Progressive apoptotic cell death triggered by transient oxidative insult in H9c2 rat ventricular cells: a novel pattern of apoptosis and the mechanisms, Am. J. Physiol. Heart Circ. Physiol. 286 (2004) H2169–H2182, https://doi.org/10.1152/ajpheart.00199.2003.
[51] H.C. Chou, Y.W. Chen, T.R. Lee, F.S. Wu, H.T. Chan, P.C. Lyu, J.F. Timms, H. L. Chan, Proteomics study of oxidative stress and Src kinase inhibition in H9C2 cardiomyocytes: a cell model of heart ischemia-reperfusion injury and treatment, Free Radical Biol. Med. 49 (2010) 96–108, https://doi.org/10.1016/j.freeradbiomed.2010.04.001.
[52] S.P. Cousin, S.R. Hügl, C.E. Wrede, H. Kajio, M.G. Myers Jr., C.J. Rhodes, Free fatty acid-induced inhibition of glucose and insulin-like growth factor I-induced deoxyribonucleic acid synthesis in the pancreatic β-cell line INS-1, Endocrinology 142 (2001) 229–240, https://doi.org/10.1210/endo.142.1.7863.
[53] D. Dyntar, M. Eppenberger-Eberhardt, K. Maedler, M. Pruschy, H.M. Eppenberger, G.A. Spinas, M.Y. Donath, Glucose and palmitic acid induce degeneration of myofibrils and modulate apoptosis in rat adult cardiomyocytes, Diabetes 50 (2001) 2105–2113, https://doi.org/10.2337/diabetes.50.9.2105.
[54] C. Leroy, S. Tricot, B. Lacour, A. Grynberg, Protective effect of eicosapentaenoic acid on palmitate-induced apoptosis in neonatal cardiomyocytes, Biochim.

Biophys. Acta Mol. Cell Biol. Lipids 1781 (2008) 685–693, https://doi.org/10.1016/j.bbalip.2008.07.009.
[55] A. Turku, M.K. Rinne, G. Boije Af Gennäs, H. Xhaard, D. Lindholm, J.P. Kukkonen, Orexin receptor agonist Yan 7874 is a weak agonist of orexin/hypocretin receptors and shows orexin receptor-independent cytotoxicity, PloS One 12 (2017), e0178526, https://doi.org/10.1371/journal.pone.0178526 e0178526.
[56] S. Berthier, L. Larrouquère, P. Champelovier, E. Col, C. Lefebvre, C. Cottet-Rouselle, J. Arnaud, C. Garrel, F. Laporte, J. Boutonnat, P. Faure, F. Hazane-Puch, A new patient-derived metastatic glioblastoma cell line: characterisation and response to sodium selenite anticancer agent, Cancers 11 (2019) 12, https://doi.org/10.3390/cancers11010012.
[57] L. Sirghi, J. Ponti, F. Broggi, F. Rossi, Probing elasticity and adhesion of live cells by atomic force microscopy indentation, Eur. Biophys. J. 37 (2008) 935–945, https://doi.org/10.1007/s00249-008-0311-2.
[58] Y.T. Zhou, P. Grayburn, A. Karim, M. Shimabukuro, M. Higa, D. Baetens, L. Orci, R. H. Unger, Lipotoxic heart disease in obese rats: implications for human obesity, Proc. Natl. Acad. Sci. U. S. A 97 (2000) 1784–1789, https://doi.org/10.1073/pnas.97.4.1784.
[59] H.C. Chiu, A. Kovacs, D.A. Ford, F.F. Hsu, R. Garcia, P. Herrero, J.E. Saffitz, J. E. Schaffer, A novel mouse model of lipotoxic cardiomyopathy, J. Clin. Invest. 107 (2001) 813–822, https://doi.org/10.1172/JCI10947.
[60] M. Kawaguchi, T. Asakura, F. Saito, O. Nemoto, K. Maehara, K. Miyake, N. Sugai, Y. Maruyama, Changes in diameter size and F-actin expression in the myocytes of patients with diabetes and streptozotocin-induced diabetes model rats, J. Cardiol. 34 (1999) 333–339. https://pubmed.ncbi.nlm.nih.gov/10642930.
[61] T. Yu, J.L. Robotham, Y. Yoon, Increased production of reactive oxygen species in hyperglycemic conditions requires dynamic change of mitochondrial morphology, Proc. Natl. Acad. Sci. U. S. A 103 (2006) 2653–2658, https://doi.org/10.1073/pnas.0511154103.
[62] S. Boudina, E.D. Abel, Diabetic cardiomyopathy, causes and effects, Rev. Endocr. Metab. Disord. 11 (2010) 31–39, https://doi.org/10.1007/s11154-010-9131-7.
[63] A. Frustaci, J. Kajstura, C. Chimenti, I. Jakoniuk, A. Leri, A. Maseri, B. Nadal-Ginard, P. Anversa, Myocardial cell death in human diabetes, Circ. Res. 87 (2000) 1123–1132, https://doi.org/10.1161/01.res.87.12.1123.
[64] F. Fiordaliso, B. Li, R. Latini, E.H. Sonnenblick, P. Anversa, A. Leri, J. Kajstura, Myocyte death in streptozotocin-induced diabetes in rats in angiotensin II-dependent, Laboratory Investigation, a Journal of Technical Methods and Pathology 80 (2000) 513–527, https://doi.org/10.1038/labinvest.3780057.
[65] B. Huisamen, M.F. Essop, R. Johnson, Phenylpyruvic acid-2-O-β-D glucoside attenuates high glucose-induced apoptosis in H9c2 cardiomyocytes, Planta Med. (2016) 1468–1474, https://doi.org/10.1055/s-0042-110856.
[66] S.F. Kemeny, D.S. Figueroa, A.M. Clyne, Hypo- and hyperglycemia impair endothelial cell actin alignment and nitric oxide synthase activation in response to shear stress, PloS One 8 (2013), e66176, https://doi.org/10.1371/journal.pone.0066176 e66176.
[67] L. Wang, T. Chen, X. Zhou, Q. Huang, C. Jin, Atomic force microscopy observation of lipopolysaccharide-induced cardiomyocyte cytoskeleton reorganization, Micron 51 (2013) 48–53, https://doi.org/10.1016/j.micron.2013.06.008.
[68] S.C. Lieber, N. Aubry, J. Pain, G. Diaz, S.-J. Kim, S.F. Vatner, Aging increases stiffness of cardiac myocytes measured by atomic force microscopy nanoindentation, Am. J. Physiol. Heart Circ. Physiol. 287 (2004) H645–H651, https://doi.org/10.1152/ajpheart.00564.2003.
[69] A.J. Engler, F. Rehfeldt, S. Sen, D.E. Discher, Microtissue elasticity: measurements by atomic force microscopy and its influence on cell differentiation, in: Cell Mechanics, Academic Press, 2007, pp. 521–545, https://doi.org/10.1016/S0091-679X(07)83022-6.
[70] F. Lautenschläger, S. Paschke, S. Schinkinger, A. Bruel, M. Beil, J. Guck, The regulatory role of cell mechanics for migration of differentiating myeloid cells, Proc. Natl. Acad. Sci. Unit. States Am. 106 (2009) 15696–15701, https://doi.org/10.1073/pnas.0811261106.
[71] S. Suresh, Biomechanics and biophysics of cancer cells, Acta Biomater. 3 (2007) 413–438, https://doi.org/10.1016/j.actbio.2007.04.002.
[72] C. Zhu, G. Bao, N. Wang, Cell mechanics: mechanical response, cell adhesion, and molecular deformation, Annu. Rev. Biomed. Eng. 2 (2000) 189–226, https://doi.org/10.1146/annurev.bioeng.2.1.189.
[73] G. Bao, S. Suresh, Cell and molecular mechanics of biological materials, Nat. Mater. 2 (2003) 715–725, https://doi.org/10.1038/nmat1001.
[74] D.A. Fletcher, R.D. Mullins, Cell mechanics and the cytoskeleton, Nature 463 (2010) 485–492, https://doi.org/10.1038/nature08908.
[75] S.G. Shroff, D.R. Saner, R. Lal, Dynamic micromechanical properties of cultured rat atrial myocytes measured by atomic force microscopy, Am. J. Physiol. 269 (1995) C286–C292, https://doi.org/10.1152/ajpcell.1995.269.1.C286.